J|A|C|S ARTICLES

Published on Web 05/01/2009

Charge Conduction and Breakdown Mechanisms in Self-Assembled Nanodielectrics

Sara A. DiBenedetto, Antonio Facchetti,* Mark A. Ratner,* and Tobin J. Marks*

Department of Chemistry and the Materials Research Center, Northwestern University, Evanston, Illinois 60208-3113

Received February 26, 2009; E-mail: a-facchetti@northwestern.edu; ratner@northwestern.edu; t-marks@northwestern.edu

Abstract: Developing alternative high dielectric constant (k) materials for use as gate dielectrics is essential for continued advances in conventional inorganic CMOS and organic thin film transistors (OTFTs). Thicker films of high-k materials suppress tunneling leakage currents while providing effective capacitances comparable to those of thin films of lower-k materials. Self-assembled monolayers (SAMs) and multilayers offer attractive options for alternative OTFT gate dielectrics. One class of materials, organosilane-based self-assembled nanodielectrics (SANDs), has been shown to form robust films with excellent insulating and surface passivation properties, enhancing both organic and inorganic TFT performance and lowering device operating voltages. Since gate leakage current through the dielectric is one factor limiting continued TFT performance improvements, we investigate here the current (voltage, temperature) (I (V,T)) transport characteristics of SAND types **II** (π-conjugated layer) and **III** (σ-saturated + π-conjugated layers) in Si/native SiO_2/SAND/Au metal−insulator−metal (MIS) devices over the temperature range −60 to +100 °C. It is found that the location of the π-conjugated layer with respect to the Si/SiO_2 substrate surface in combination with a saturated alkylsilane tunneling barrier is crucial in controlling the overall leakage current through the various SAND structures. For small applied voltages, hopping transport dominates at all temperatures for the π-conjugated system (type **II**). However, for type **III** SANDs, the σ- and π- monolayers dominate the transport in two different transport regimes: hopping between +25 °C and +100 °C, and an apparent switch to tunneling for temperatures below 25 °C. The σ-saturated alkylsilane tunneling barrier functions to reduce type **III** current leakage by blocking injected electrons, and by enabling bulk-dominated (Poole−Frenkel) transport vs electrode-dominated (Schottky) transport in type **II** SANDs. These observations provide insights for designing next-generation self-assembled gate dielectrics, since the bulk-dominated transport resulting from combining σ- and π-layers should enable realization of gate dielectrics with further enhanced performance.

Introduction

It is well-accepted that the SiO_2 gate dielectric layer for sub-0.1 μm MOSFETs (metal oxide semiconductor field effect transistors) has a minimum practical thickness of ~3 nm.[1] Below this limit, (gate) tunneling currents cannot be neglected since they are as large as 10^{-3} A/cm^2 at 1.0 V.[2,3] For more than four decades, the semiconductor industry has relied on manipulation of poly-silicon and SiO_2 thicknesses to achieve advances in microprocessor performance every 24 months. It was not until one year ago that computer chips (based on 45-nm CMOS technology) incorporated a *new* gate stack, which for the first time integrated a high-k oxide (HfO_2) gate dielectric into CMOS production. By utilizing a high-k dielectric, thicker dielectric films and reduced gate tunneling leakage currents can be achieved without reducing the effective capacitance of the gate stack. The switch to new dielectric (and gate) materials has been heralded as "the biggest change in transistor technology since the late 1960's".[4] However, as MOSFETs are scaled to even smaller dimensions, the requisite reduction in dielectric thickness has already led to increased leakage currents.[5] For example, 9 nm of HfO_2 deposited by atomic layer deposition (ALD) on InGaAs at 250 °C exhibits $J \approx 10^{-5}$ A/cm^2 at 2.0 V, which can be reduced to 10^{-6} A/cm^2 by surface passivation with H_2S prior to HfO_2 deposition.[6] In another example, 3.5 nm of HfO_2 deposited by electron-beam evaporation at 150 °C on Si(100), exhibits $J \approx 10^{-4}$ A/cm^2 at 1.0 V.[7] Leakage current values of this magnitude are far too large for organic thin film transistor (OTFT) applications, where typical device currents are on the same order as these leakage currents (consult the literature[8−14] for OTFT device operation and background information). For

(1) Depas, M.; Van Meirhaeghe, R. L.; Laflere, W. H.; Cardon, F. *Solid-State Electron.* **1994**, *37*, 433–441.
(2) Boulas, C.; Davidovits, J. V.; Rondelez, F.; Vuillaume, D. V. *Microelect. Eng.* **1995**, *1995*, 217–220.
(3) Osada, M.; Ebina, Y.; Funakubo, H.; Yokoyama, S.; Kiguchi, T.; Takada, K.; Sasaki, T. *Adv. Mater.* **2006**, *18*, 1023–1027.
(4) Bohr, M. T.; Chau, R. S.; Ghani, T.; Mistry, K. *IEEE Spect.* **2007**, *10*, 29.
(5) Hu, H.; Zhu, C.; Lu, Y. F.; Li, M. F.; Cho, B. J.; Choi, W. K. *IEEE Elec. Dev. Lett.* **2002**, *23*, 514.
(6) O'Connor, E.; Long, R. D.; Cherkaoui, K.; Thomas, K. K.; Chalvet, F.; Povey, I. M.; Pemble, M. E.; Hurley, P. K.; Brennan, B.; Hughes, G.; Newcomb, S. B. *Appl. Phys. Lett.* **2008**, *92*, 022902.
(7) Cherkaoui, K.; Monaghan, S.; Negara, M. A.; Modreanu, M.; Hurley, P. K.; O'Connell, D.; McDonnell, S.; Wright, S. B., R. C.; Bailey, P.; Noakes, T. C. Q. *J. Appl. Phys.* **2008**, *104*, 064113.
(8) Kitamura, M.; Arakawa, Y. *J. Phys.: Condens. Matter* **2008**, *20*, 184011.

 10.1021/ja9013166 CCC: $40.75 © 2009 American Chemical Society

these reasons, the current industrial interest in alternative dielectric materials presents an opportunity for the organic dielectrics/electronics community, where the nanoscale fabrication of pristine films of self-assembled monolayers (SAMs) and multilayers (SAMTs) is now well advanced.[15−20]

As an example, mono- and dithiols of saturated alkanes (and their conjugated aromatic counterparts) form densely packed and well-ordered domains of up to several hundred square nanometers in dimensions on Au, Ag,[21−24] Cu,[25−27] Pd,[19,28] and Pt[29,30] substrates. In addition, *n*-alkanoic acids, phosphonic acids, and organosilane molecules ($RSiX_3$, with X = Cl, OMe, OEt) form SAMs on hydroxylated substrate surfaces such as Si/SiO_2, Al/Al_2O_3, and tin-doped indium oxide (ITO).[31−33] Our group has reported on the electrical properties of self-assembled nanodielectrics (SANDs) in MIS (metal−insulator−semiconductor) capacitors, and as gate dielectrics in OTFTs.[34] Originally we reported three types of SAND structures (**I**, **II**, and **III**), each fabricated via a layer-by-layer solution phase self-assembly of $\sigma-\pi$ silane molecular precursors to form hybrid organic−inorganic (SiO_2) multilayers (Figure 1). Type **II** consists of conjugated organic dye molecule (**Stb**) and SiO_2 **Cap** layers, while type **III** is built up of multiple monolayers of different constituents in the following order: **C8** alkyl + siloxane **Cap** + **Stb** π-dye + siloxane **Cap**. Note that type **I** consists of a **C8** alkyl monolayer and a SiO_2 **Cap** layer (bottom portion of **III**).

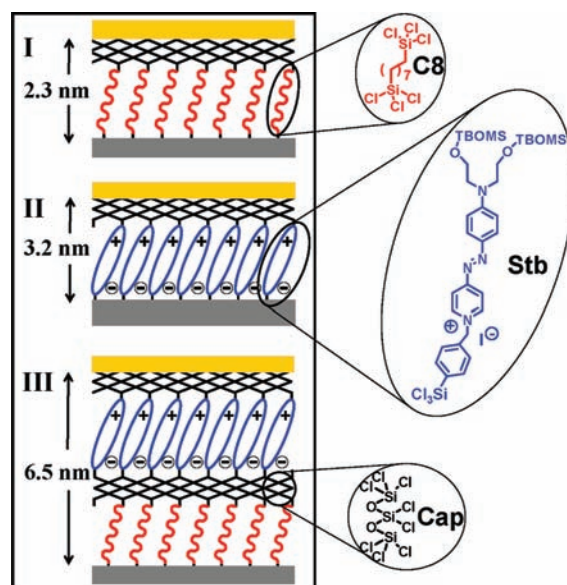

Figure 1. Chemical components of the SAND family illustrated in Si/SiO_2/SAND/Au MIS devices. SAND type **I** consists of two monolayers: **C8** and **Cap**, and similarly SAND type **II** consists of two monolayers: **Stb** and **Cap**. SAND type **III** is composed of multiple monolayers in the following order **C8** + **Cap** + **Stb** + **Cap**. The thicknesses of types **II** and **III** are measured by X-ray reflectivity (Figure S1), and the thickness of types **I** was reported previously.[34]

These specialized SAMTs exhibit excellent insulating and dielectric properties including: large measured breakdown fields (~5−7 $MVcm^{-1}$), large capacitances (C_i = 400 (**I**); 710 (**II**); 390 (**III**) nF/cm^2 at 10^2 Hz), low leakage currents (~10^{-8}−10^{-5} A/cm^2 at 1 V), and enable low operating voltage p-type and n-type OTFTs.[34]

An alternative semiconductor technology to Si/SiO_2 has focused on using III−V compound semiconductors such as GaAs.[35,36] However, the main obstacle to large-scale commercialization has been the lack of compatible gate dielectrics and electrical passivation layers for the efficient modulation of the GaAs channel.[6] We recently demonstrated an advance in GaAs surface passivation, where GaAs metal−insulator−semiconductor field-effect transistors (MISFETs) used SANDs as the gate dielectric.[37] Devices exhibited 10^{-5} A/cm^2 gate leakage current densities at ~3 V, and very small (<80 mV) hysteresis in capacitance−voltage scans.

These MISFET performance characteristics indicate few interfacial traps upon surface modification with SANDs. Recently, it was shown that the performance of GaAs junction field effect transistors (JFETs) is also improved by incorporating type **I** or **III** SANDs as gate dielectrics versus control devices using 1-octadecanethiol (ODT) monolayers.[38] The interfaces in the GaAs/**I** and GaAs/**III** structures both contain an **Alk** layer directly bound to the hydroxylated GaAs surface. However, junction field effect transistors with type **III** exhibit superior passivation (lower subthreshold slope) and negative threshold

(9) Allard, S.; Forster, M.; Souharce, B.; Thiem, H.; Scherf, U. *Angew. Chem., Int. Ed.* **2008**, *47*, 4070.
(10) Di, C.-A.; Yu, G.; Liu, Y.; Zhu, D. *J. Phys. Chem. B* **2007**, *111*, 14083.
(11) Facchetti, A. *Mater. Today* **2007**, *10*, 28.
(12) Zaumseil, J.; Sirringhaus, H. *Chem. Rev.* **2007**, *107*, 1296.
(13) Newman, C. R.; Frisbie, C. D.; Filho, D. A. d. S.; Bredas, J.-L.; Ewbank, P. C.; Mann, K. R. *Chem. Mater.* **2004**, *16*, 4436.
(14) Dimitrakopoulos, C. D.; Malenfant, P. R. L. *Adv. Mater.* **2002**, *14*, 99.
(15) Sagiv, J. *J. Am. Chem. Soc.* **1980**, *10*, 92.
(16) Ulman, A. *An Introduction to Ultrathin Organic Films from Langmuir-Blodgett to Self-Assembly*; Academic Press: San Diego, 1991.
(17) Poirier, G. E.; Pylant, E. D. *Science* **1996**, *272*, 1145.
(18) Schreiber, F. *J. Phys.: Condens. Matter* **2004**, *16*, R881.
(19) Love, J. C.; Wolfe, D. B.; Haasch, R.; Chabinyc, M. L.; Paul, K. E.; Whitesides, G. M.; Nuzzo, R. G. *J. Am. Chem. Soc.* **2003**, *125*, 2597.
(20) Aswal, D. K.; Lenfant, S.; Guerin, D.; Yakhmi, J. V.; Vuillaume, D. *Anal. Chim. Acta* **2006**, *568*, 84.
(21) Rusu, P. C.; Giovannetti, G.; Brocks, G. *J. Phys. Chem. C* **2007**, *111*, 14448.
(22) Laibinis, P. E.; Whitesides, G. M.; Allara, D. L.; Tao, Y. T.; Parikh, A. N.; Nuzzo, R. G. *J. Am. Chem. Soc.* **1991**, *113*, 7152.
(23) Weiss, E. A.; Chiechi, R. C.; Kaufman, G. K.; Kriebel, J. K.; Li, Z.; Duati, M.; Rampi, M. A.; Whitesides, G. M. *J. Am. Chem. Soc.* **2007**, *129*, 4336.
(24) Shaporenko, A.; Ulman, A.; Zharnikov, M. *J. Phys. Chem. B* **2005**, *109*, 3898.
(25) Hoque, E.; DeRose, J. A.; Houriet, R.; Hoffmann, P.; Mathieu, H. J. *Chem. Mater.* **2007**, *19*, 798.
(26) Jennings, G. K.; Yong, T.-H.; Munro, J. C.; Laibinis, P. E. *J. Am. Chem. Soc.* **2003**, *125*, 2950.
(27) Vollmer, S.; Witte, G.; Woell, C. *Langmuir* **2001**, *17*, 7560.
(28) Stapleton, J. J.; Daniel, T. A.; Uppili, S.; Cabarcos, O. M.; Naciri, J.; Shashidhar, R.; Allara, D. L. *Langmuir* **2005**, *21*, 11061.
(29) Noguchi, H.; Ito, M.; Uosaki, K. *Chem. Lett.* **2005**, *34*, 950.
(30) Lee, S.; Park, J.; Ragan, R.; Kim, S. H.; Lee, Z.; Lim, D. K.; Ohlberg, D. A. A.; Williams, R. S. *J. Am. Chem. Soc.* **2006**, *128*, 5745.
(31) Haensch, C.; Ott, C.; Hoeppener, S.; Schubert, U. S. *Langmuir* **2008**, *24*, 10222.
(32) Cui, J.; Huang, Q.; Veinot, J. C. G.; Yan, H.; Wang, Q.; Hutchison, G. R.; Richter, A. G.; Evmenenko, G.; Dutta, P.; Marks, T. J. *Langmuir* **2002**, *18*, 9958.
(33) Li, J.; Lui, J.; Evmenenko, G. A.; Dutta, P.; Marks, T. J. *Langmuir* **2008**, *24*, 5755.
(34) Yoon, M.-H.; Facchetti, A.; Marks, T. J. *Proc. Natl. Acad. Sci.* **2005**, *102*, 4678.
(35) Razeghi, M. *IEEE J. Sel. Top. Quant. Electron.* **2000**, *6*, 1344.
(36) McGuiness, C. L.; Blasini, D.; Masejewski, J. P.; Uppili, S.; Cabarcos, O. M.; Smilgies, D.; Allara, D. L. *Am. Chem. Soc. Nano* **2007**, *1*, 30.
(37) Lin, H. C.; Ye, P. D.; Xuan, Y.; Facchetti, A.; Marks, T. J. *Appl. Phys. Lett.* **2006**, *89*, 142101.
(38) Lee, K.; Lu, G.; Facchetti, A.; Janes, D. B.; Marks, T. J. *Appl. Phys. Lett.* **2008**, *92*, 123509.

voltage (V_T) shifts compared to devices with ODT or SAND type **I**, which exhibit positive V_T shifts. These improvements were tentatively attributed to the fixed charges associated with the negative I^- counterions contained in the **Stb** molecular layer. It was proposed that these fixed charges create a strong local electric field oriented toward the underlying GaAs surface, which is essential to enhance GaAs junction field effect transistor performance.[38] The results of these studies motivate the present investigation of charge injection and leakage current transport mechanisms through SAND types **II** and **III** dielectrics, enabling the comparison of electron injection and transport through nanoscopic π-conjugated vs σ-saturated gate dielectric systems.

In the transport/molecular electronics community, σ- vs π-conduction pathway distinctions are important since it is known that the smaller HOMO−LUMO gaps of π-conjugated molecules (~3 eV) enhance charge transport as compared to the larger gaps of σ-saturated molecules (6−8 eV).[39−43] Furthermore, from the tunneling model (eq 1a), the tunneling decay parameter (β, eq 1b)[44] for

$$J(d) = J_o \exp(-\beta d) \tag{1a}$$

$$\beta = \frac{4\pi(2m\phi)^{1/2}}{h}\alpha \tag{1b}$$

π-conjugated molecules is accepted to be 0.2−0.6 Å^{-1}, compared to ~0.6−1.2 Å^{-1} for σ-saturated molecules.[45] Here J is the leakage current density, J_o is the low field conductivity, d is the thickness of the insulator (or SAM), ϕ is the tunneling barrier, h is Planck's constant, m is the electron mass, and α is a unitless parameter describing the asymmetry of the potential profile ($\alpha = 1$ for a rectangular barrier). The lower β values for π-conjugated molecules indicate more efficient tunneling due to π-orbital delocalization over the molecule.[45−48] Furthermore, it is well documented that polar SAMs can tune the electronic properties of their interfaces with semiconductors/metals by shifting the surface potential/dipole,[49−53] carrier density,[54−56] electron affinity,[57−60] and work function.[61−66] Due to the inherent differences between σ- and π-type systems, it has been suggested that extended π-conjugated molecules may prefer hopping as the dominant transport mechanism rather than tunneling.[45,67,68] Note that charge transport in SAMs is very sensitive to the nature of the contact, and thus the conduction mechanism for SAMs grown on oxide surfaces is far less understood than for SAMs on Au.[69−71] As an example, one recent study investigated transport in 3-aminoproplytrimethoxysilane SAMTs,[72] and hopping was suggested to be the dominant transport mechanism (rather than tunneling) on the basis of the nonexponential thickness dependence of the current density. However, the mechanism was not further investigated with temperature-dependent $I-V$ studies. Thus, as conjugated SAM(T)s become more widely used in TFTs and other devices,[73] it is important to elucidate the influences of smaller HOMO−LUMO gaps and larger dipole moments on transport through SAM(T)s for insight into the design of next-generation robust, molecular self-assembled gate dielectrics.[51,74,75] In the present investigation, the $I(V,T)$ data are acquired and analyzed for hopping vs tunneling transport at low voltages, and for injection/emission transport at normal OFET operating voltages (intermediate voltage range 2.0−3.0 V). Finally, the large voltage SAND dielectric breakdown barriers are presented and discussed. Instead of the common thickness dependent transition between tunneling and hopping observed for single molecule electronic junctions, it will be seen here that microstructural differences between types **II** and **III** (π-conjugated layer vs σ-saturated + π-conjugated layers, and the location of I^- counterion) largely determine the different operative conduction mechanisms.

Experimental Methods

SAND films on heavily doped n^+-Si substrates were fabricated as reported previously.[34] The thicknesses of type **II** and type **III**

(39) Ratner, M. A.; Davis, B.; Kemp, M.; Mujica, V.; Roitberg, A.; Yaliraki, S. *In Molecular Electronics*; Aviram, A., Ratner, M. A., Eds.; New York Academy of Sciences: New York, 1998; Vol. 852.
(40) Wang, W.; Lee, T.; Reed, M. A. *J. Phys. Chem. B* **2006**, *108*, 18398.
(41) McCreery, R. L. *Chem. Mater.* **2004**, *16*, 4477.
(42) Bock, C.; Pham, D. V.; Kunze, U.; Kafer, D.; Witte, G.; Woll, C. *J. Appl. Phys.* **2006**, *100*, 114517.
(43) Kim, B.; Beebe, J. M.; Jun, Y.; Zhu, X.-Y.; Frisbie, C. D. *J. Am. Chem. Soc.* **2006**, *128*, 4970.
(44) Wang, W.; Takhee, L.; Reed, M. A. *Phys. Rev. B* **2003**, *68*, 035416.
(45) Salomon, A.; Cahen, D.; Lindsay, S.; Tomfohr, J.; Engelkes, V. B.; Frisbie, C. D. *Adv. Mater.* **2003**, *15*, 1881.
(46) James, D. K.; Tour, J. M. *Chem. Mater.* **2004**, *16*, 4423.
(47) Akkerman, H. B.; de Boer, B. *J. Phys.: Condens. Matter* **2008**, *20*, 013001.
(48) Wold, D. J.; Haag, R.; Rampi, M. A.; Frisbie, C. D. *J. Phys. Chem. B* **2002**, *106*, 2813.
(49) Miramond, C.; Vuillaume, D. *J. Appl. Phys.* **2004**, *96*, 1529.
(50) Kera, S.; Yabuuchi, Y.; Yamane, H.; Setoyama, H.; Okudaira, K. K.; Kahn, A.; Ueno, N. *Phys. Rev. B* **2004**, *70*, 085304.
(51) Scott, A.; Janes, D. B.; Risko, C.; Ratner, M. A. *Appl. Phys. Lett.* **2007**, *91*, 033508.
(52) Haick, H.; Ambrico, M.; Ligonzo, T.; Tung, R. T.; Cahen, D. *J. Am. Chem. Soc.* **2006**, *128*, 6854.
(53) Ray, S. G.; Cohen, H.; Naaman, R.; Liu, H.; Waldeck, D. H. *J. Phys. Chem. B* **2005**, *109*, 14064.
(54) Kobayashi, S.; Nishikawa, T.; Takenobu, T.; Mori, S.; Shimoda, T.; Mitani, T.; Shimotani, H.; Yoshimoto, N.; Ogawa, S.; Iwasa, A. *Nat. Mater.* **2004**, *3*, 317.
(55) Heimel, G.; Romaner, L.; Zojer, E.; Bredas, J.-L. *Nano Lett.* **2007**, *7*, 932.
(56) Huang, C.; Katz, H. E.; West, J. E. *Langmuir* **2007**, *23*, 13223.
(57) Gershewitz, O.; Grinstein, M.; Sukenik, C. N.; Regev, K.; Ghabboun, J.; Cahen, D. *J. Phys. Chem. B* **2004**, *108*, 664.
(58) Lenfant, S.; Guerin, D.; Tran Van, F.; Chevrot, C.; Palacin, S.; Bourgoin, J. P.; Bouloussa, O.; Rondelez, F.; Vuillaume, D. *J. Phys. Chem. B* **2006**, *110*, 13947.
(59) Peor, N.; Sfez, R.; Yitzchaik, S. *J. Am. Chem. Soc.* **2008**, *130*, 4158.
(60) Cohen, R.; Kronik, L.; Shanzer, A.; Cahen, D.; Liu, A.; Rosenwaks, Y.; Lorenz, J. K.; Ellis, A. B. *J. Am. Chem. Soc.* **1999**, *121*, 10545.
(61) Ganzorig, C.; Kwak, K.-K.; Yagi, K.; Fujihira, M. *Appl. Phys. Lett.* **2001**, *79*, 272.
(62) de Boer, B.; Handipour, A.; Mandoc, M. M.; van Woundenbergh, T.; Blom, P. W. M. *Adv. Mater.* **2005**, *17*, 621.
(63) Demirkan, K.; Matthew, A.; Weiland, C.; Yao, Y.; Rawlett, A. M.; Tour, J. M.; Opila, R. L. *J. Chem. Phys.* **2008**, *128*, 074705.
(64) Katz, H. E.; Johnson, J.; Lovinger, A. J.; Li, W. *J. Am. Chem. Soc.* **2000**, *122*, 7787.
(65) Vazquez, H.; Gao, W.; Flores, F.; Kahn, A. *Phys. Rev. B Rapid Commun* **2005**, *71*, 041306.
(66) Ishii, H.; Sugiyama, K.; Ito, E.; Seki, K. *Adv. Mater.* **1999**, *11*, 605.
(67) Holmlin, R. E.; Haag, R.; Chabinyc, M. L.; Ismagilov, R. F.; Cohen, A. E.; Terfort, A.; Rampi, M. A.; Whitesides, G. M. *J. Am. Chem. Soc.* **2001**, *123*, 5075.
(68) Tran, E.; Duati, M.; Ferri, V.; Müllen, K.; Zharnikov, M.; Whitesides, G. M.; Rampi, M. A. *Adv. Mater.* **2006**, *18*, 1323.
(69) Boulas, C.; Davidovits, J. V.; Rondelez, F.; Vuillaume, D. *Phys. Rev. Lett.* **1996**, *76*, 4797.
(70) Selzer, Y.; Salomon, A.; Cahen, D. *J. Phys. Chem. B* **2002**, *106*, 10432.
(71) Gu, Y.; Akhremitchev, B.; Walker, G. C.; Waldeck, D. H. *J. Phys. Chem. B* **1999**, *103*, 5220.
(72) Chauhan, A. K.; Aswal, D. K.; Koiry, S. P.; Gupta, S. K.; Yakjmi, J. V.; Suergers, C.; Guerin, D.; Lenfant, S.; Vuillaume, D. *Appl. Phys. A: Mater. Sci. Proc.* **2008**, *90*, 581.
(73) DiBenedetto, S. A.; Facchetti, A.; Ratner, M. A.; Marks, T. J. *Adv. Mater.* **2009**, *21*, 1407.
(74) Salomon, A.; Shapaisman, H.; Seitz, O.; Boecking, T.; Cahen, D. *J. Phys. Chem. C* **2008**, *112*, 3969.
(75) Kalakodimi, R. P.; Nowak, A. M.; McCreery, R. L. *Chem. Mater.* **2005**, *17*, 4939.

SAND films were determined by specular X-ray reflectivity[76] measurements (Figure S1). The MIS devices were completed by vapor deposition of patterned Au electrodes (50 nm thick, 10^{-7} Torr, 0.02 Å/s for the first 10 nm, then 0.3 Å/s up to 50 nm) through a shadow mask with an electrode area of 200 × 200 μm^2. Direct current (I) as a function of voltage (V) was measured in the dark, under vacuum (~6 × 10^{-6} Torr), and over a wide temperature range (−60 to +100 °C). Two-probe electrical $I-V$ measurements were performed with a Keithley 6430 Sub-Femtoamp remote source meter operated by a local LABVIEW program. Triaxial and low triboelectric noise coaxial cables were incorporated with the Keithley remote source meter and Signatone (Gilroy, CA) probe tip holders to minimize the noise level. The leakage current densities (J, A/cm^2) were measured with positive/negative polarity applied to the Au electrode to ensure the n^+-Si substrate was operated in accumulation. Long delay times of 2−6 s were incorporated into the source−delay−measure cycle to ensure that the source was settled before recording currents.

The Heli-Tran Open Cycle cryostat and LT3B−110 coldend were purchased from Advanced Research Systems (Macungie, PA) and adapted to the high-vacuum chamber. Device substrates and the silicon diode used to record the temperature were mounted on a 1.0 mm-thick sapphire crystal, attached to the cryostat sample stage with indium. The temperature range used in this study was achieved with liquid nitrogen as the cryogen, and the temperature was controlled using a LakeShore (Westerville, OH) model 332 temperature controller equipped with dual calibrated silicon diode temperature sensors. The cold stage was partially covered with a radiation shield to further control heat losses. Calibration of the sample temperature was performed using a surface thermocouple mounted on top of a clean Si substrate (attached to the coldend in the same configuration as the SAND samples). The temperature of the Si surface was recorded after 15 min to ensure thermal equilibrium at each temperature step, and the temperature readings were found to be in good agreement with the silicon diode mounted on the coldend.

Theoretical Considerations

There is abundant literature on SAM conduction mechanisms[77−81] and charge transport;[20,41,45−47,82−86] therefore, this section focuses on some of the most discussed conduction mechanisms.

1. Tunneling. Nonresonant tunneling (through space) is the most common transport mechanism observed in saturated alkyl SAMs.[87−94] However, for π-conjugated molecular SAMs, near-resonant tunneling through the molecular orbitals may also occur due to the smaller HOMO−LUMO gap.[70,95−97] The simplest tunneling model assumes a finite potential barrier at the metal−insulator interface and describes the finite probability that electrons can travel a short distance into the SAM (or insulator), despite the lack of available energy levels. This process is given by the Simmons relation (eq 2), which is expressed here in the simplest form (a rectangular barrier) to emphasize the exponential dependence of the current density (J_{DT}) on the thickness (d) and barrier height (ϕ),[20,41]

$$J_{DT} = \frac{q^2V}{h^2d}(2m^*\phi)^{1/2}\exp\left(\frac{-4\pi d}{h}(2m^*\phi)^{1/2}\right) \quad (2)$$

where q is the electron charge, V is the applied voltage, m^* is the effective electron mass in the dielectric, and the other terms have been defined previously. For very large applied voltages ($V > \phi$), the barrier changes to a triangular shape, and the tunneling current is given by the Fowler−Nordheim (F−N) equation (eq 3).[20,98−101]

$$J_{FN} = \frac{q^3E^2}{16\pi^2\hbar m^*\phi_{FN}}\exp\left(-\frac{4\sqrt{2m^*}}{3q\hbar E}(\phi_{FN})^{3/2}\right) \quad (3)$$

Here ϕ_{FN} is the tunneling barrier height, E is the electric field (V/d), and m^* is the effective electron mass. F−N emission has the strongest dependence on the applied voltage but is essentially independent of the temperature.

2. Hopping. Hopping refers to ohmic transport, which is dominant for thicker layers at low fields and moderate temperatures. Simple hopping follows a classical Arrhenius relation (eq 4),[79,102]

$$\sigma = \sigma_0 \exp\left(\frac{-E_a}{kT}\right) \quad (4)$$

where σ is the conductivity ($\sigma = J/E$, and $E = V/d$), k is the Boltzmann constant, and E_a is the activation energy. McCreery et al.[41] associated hopping with nuclear motion (or molecular reorganization), whereas Bässler et al.[103−105] proposed that hopping occurs among large defects or impurities. Whatever

(76) Zhu, P.; van der Boom, M. E.; Kang, H.; Evmenenko, G.; Dutta, P.; Marks, T. J. *Chem. Mater.* **2002**, *14*, 4982.
(77) O'Dwyer, J. *Theory of Electrical Conduction and Breakdown in Solid Dielectrics*; Clarendon Press: Oxford, 1973.
(78) Simmons, J. G. *J. Phys. D: Appl. Phys.* **1971**, *4*, 613.
(79) Sze, S. M. *Physics of Semiconductor Devices*, 2nd ed.; John Wiley and Sons: New York, 1981.
(80) Davis, J. J.; Wang, N.; Morgan, A.; Zhang, T.; Zhao, J. *Faraday Discuss.* **2006**, *131*, 167.
(81) Weiss, E. A.; Chiechi, R. C.; Kaufman, G. K.; Kriebel, J. K.; Li, Z.; Duati, M.; Rampi, M. A.; Whitesides, G. M. *J. Am. Chem. Soc.* **2007**, *129*, 4336.
(82) Berlin, Y. A.; Burin, A. L.; Ratner, M. A. *Chem. Phys.* **2002**, *275*, 61.
(83) Wang, W.; Lee, T.; Reed, M. A. *Proc. IEEE* **2005**, *95*, 1815.
(84) Chabinyc, M. L.; Chen, X.; Holmlin, R. E.; Jacobs, H.; Skulason, H.; Frisbie, C. D.; Mujica, V.; Ratner, M. A.; Rampi, M. A.; Whitesides, G. M. *J. Am. Chem. Soc.* **2002**, *124*, 11730.
(85) Duati, M.; Grave, C.; Tcbeborateva, N.; Jishan, W.; Mullen, K.; Shaporenko, A.; Zharnikov, M.; Kriebel, J. K.; Whitesides, G. M.; Rampi, M. A. *Adv. Mater.* **2006**, *18*, 329.
(86) Burin, A. L.; Ratner, M. A. In *Computational Materials Chemistry: Methods and Aplications*; Curtiss, L. A., Gordon, M. S., Eds.; Kluwer Academic: Netherlands, 2004; p 308.
(87) Mbindyo, J. K. N.; Mallouk, T. E.; Mattzela, J. B.; Kratochvilova, I.; Razavi, B.; Jackson, T. N.; Mayer, T. S. *J. Am. Chem. Soc.* **2002**, *124*, 4020.
(88) Mujica, V.; Ratner, M. A. *Chem. Phys.* **2001**, *264*, 365.
(89) Ulgut, B.; Abruna, H. D. *Chem. Rev.* **2008**, *108*, 2721.
(90) Tran, E.; Grave, C.; Whitesides, G. M.; Rampi, M. A. *Electrochim. Acta* **2005**, *50*, 4850.
(91) Grave, C.; Risko, C.; Shaporenko, A.; Wang, Y.; Nuckolls, C.; Ratner, M. A.; Rampi, M. A.; Zharnikov, M. *Adv. Funct. Mater.* **2007**, *17*, 3816.
(92) Maisch, S.; Effenberger, F. *J. Am. Chem. Soc.* **2005**, *127*, 17315.
(93) Shamai, T.; Ophir, A.; Selzer, Y. *Appl. Phys. Lett.* **2007**, *91*, 102108.
(94) Chen, F.; Li, X.; hihath, J.; Huang, Z.; Tao, N. *J. Am. Chem. Soc.* **2006**, *128*, 15874.
(95) Fan, F.-R. F.; Yang, J.; Cai, L.; Price, D. W.; Dirk, S. M.; Kosykin, D. V.; Yao, Y.; Rawlett, A. M.; Tour, J. M.; Bard, A. J. *J. Am. Chem. Soc.* **2002**, *124*, 5550.
(96) Akkerman, H. B.; Blom, P. W. M.; de Leeuw, D. M.; de Boer, B. *Nature* **2006**, *441*, 69.
(97) Zhitenev, N. B.; Erbe, H.; Bao, Z. *Nanotech.* **2003**, *14*, 254.
(98) Banerjee, S.; Shen, B.; Chen, I.; Bohlman, J.; Brown, G.; Doering, R. *J. Appl. Phys.* **1989**, *65*, 1140–1146.
(99) Lenzinger, M.; Snow, E. H. *J. Appl. Phys.* **1969**, *40*, 278.
(100) Beebe, J. M.; Kim, B.; Gadzuk, J. W.; Frisbie, C. D.; Kushmerick, J. G. *Phys. Rev. Lett.* **2006**, *97*, 026801.
(101) Aswal, D. K.; Lenfant, S.; Guerin, D.; Yakhmi, J. V.; Vuillaume, D. *Small* **2005**, *1*, 725.
(102) Cracium, N. I.; Wildeman, J.; Blom, P. W. M. *Phys. Rev. Lett.* **2008**, *100*, 056601.

the origin of the hopping, it is observed much less frequently in SAMs than is tunneling because the typical lengths of the molecules investigated are seldom greater than ~2 nm.[90,106,107] Extensive theoretical work has been reported concerning the tunneling→hopping transition,[82,108−114] and earlier data on some organics[115−118] and DNA[119,120] have revealed a clear length-dependent transition between tunneling and hopping conduction. Recently, this transition was demonstrated in Au−molecule−Au junctions, where the electrical resistance of oligophenyleneimine (OPI) molecules of various lengths was measured with a conductive AFM tip.[121] Hopping transport was found in OPI molecules longer than 4 nm, while molecules <4 nm in length exhibit nonresonant tunneling.

As the voltage range is increased above the low bias hopping regime, different transport mechanisms may become dominant.[122,123] Since the energy distribution of electrons in metals is given by the Fermi−Dirac distribution function, at these intermediate voltages (and higher temperatures), a larger fraction of the electrons will have sufficient energy to surmount the energetic barrier presented by the SAM. Thermionic (Schottky) emission (eq 5) assumes that an electron from the contact can be injected into the dielectric once it has acquired sufficient thermal energy to cross the potential maximum resulting from the superposition of the external and the image-charge potential.[103,124,125] However, if the SAM has structural imperfections or defect states, they can act as electron traps. In this case, the thermally excited trapped electrons will contribute to the current density according to Poole−Frenkel emission (eq 6)[78] at high temperatures and intermediate voltages.[20,98,126]

$$J_S = A^*T^2 \exp\left(\frac{-q(\phi_S - \sqrt{qE/4\pi\varepsilon\varepsilon_o})}{kT}\right) \tag{5}$$

$$J_{PF} = J_o \exp\left(\frac{-q(\phi_{PF} - \sqrt{qE/\pi\varepsilon\varepsilon_o})}{kT}\right) \tag{6}$$

Often the exponents of eqs 5 and 6 are simplified by introducing β parameters [$\beta_S = (q^3/4\varepsilon\pi_o\varepsilon)^{1/2}$ and $\beta_{PF} = (q^3/\varepsilon\pi_o\varepsilon)^{1/2}$], which correspond to the slopes of the logarithmic plots of eqs 5 and 6.[127] Both mechanisms result from Coulombic lowering of the potential barrier under an applied electric field, and the two processes have similar $J(V,T)$ dependencies except the square root in the exponential is 2× larger for Poole−Frenkel emission compared to Schottky emission. Here, A^* is the modified Richardson's constant ($A^* = 120$ A/cm^2·K^2),[78,103] E is the electric field ($E = V/d$), J_o is the low-field conductivity ($= \sigma_o E$), ϕ_S and ϕ_{PF} are the Schottky and Poole−Frenkel barrier heights, respectively, ε is the dielectric permittivity, ε_o is the permittivity of vacuum, and k the Boltzmann constant.[79]

Results

First, we investigate the low voltage transport mechanism from the SAND $I(V,T)$ data displayed in an Arrhenius format. On the basis of these first observations, the remainder of the results are organized into two different transport regimes: (i) high temperatures >25 °C and (ii) low temperatures <25 °C. First, the high temperature transport is analyzed over an intermediate voltage range by using standard emission models, followed by analysis of data in the large voltage, field-induced tunneling regime. Second, the low-temperature $I(V,T)$ data for type **III** SANDs are examined using the Simmons equation for tunneling. Finally, in the Discussion, we present a full comparative analysis of the current leakage and dielectric breakdown characteristics of the type **II** and **III** SANDs.

We first investigate the transport characteristics of SANDs **II** and **III** in MIS devices as a function of temperature. For nonbreakdown analysis (low voltages), the $I-V$ traces of Si/native SiO_2/SAND/Au MIS devices were obtained over the ranges ±1.0 V for type **II** and ±2.0 V for type **III**. It has been suggested that hopping dominates transport through organosilane SAMs on Si/SiO_2 substrates at low voltages.[69,70] Figure 2 shows the temperature dependence of SAND **II** and **III** resistance (determined from the slope of the $I-V$ curve around zero) plotted according to the standard Arrhenius equation (eq 4); see Supporting Information Figure S2 for an alternative representation as R (Ω) vs T (K).

Figure 2 shows that the resistance (R) vs inverse temperature ($1/T$) of type **II** and type **III** SANDs follow similar trends at high temperatures, despite a priori expectations based on the thicknesses: d(**II**) = 3.2 nm is within the typical range for tunneling, and d(**III**) = 6.5 nm is within the typical range for hopping. While thickness dependent tunneling to hopping transport evolution is not observed within this measurement range for SANDs, Figure 2 does reveal an apparent *temperature-dependent* change in transport mechanism for type **III**. The nearly temperature independent behavior observed in **III** over the low temperature range (from −60 to −10 °C) implicates tunneling, whereas the activated region over the high temperature range (from 25 to 100 °C) implies hopping. The activation energies determined via linear regression analysis are 0.13 ± 0.02 eV for

(103) Barth, S.; Wolf, U.; Bassler, H.; Muller, P.; Riel, H.; Vestweber, H.; Seidler, P. F.; Reiss, W. *Phys. Rev. B* **1999**, *60*, 8791.
(104) Lampert, M. A.; Mark, P. *Current Injection in Solids*; Academic Press: New York, 1970.
(105) Pope, M.; Swenberg, C. E. *Electronic Processes In Organic Crystals and Polymers*, 2nd ed.; Oxford University Press: New York, 1999.
(106) Selzer, Y.; Cabassi, M. A.; Mayer, T. S.; Allara, D. L. *Nanotech.* **2004**, *15*, S483.
(107) Segal, D.; Nitzan, A.; Ratner, M. A.; Davis, W. B. *J. Phys. Chem. B* **2000**, *104*, 2790.
(108) Lakhno, V. D.; Sultanov, V. B.; Pettitt, B. M. *Chem. Phys. Lett.* **2004**, *400*, 47.
(109) Renger, T.; Marcus, R. A. *J. Phys. Chem. A* **2003**, *107*, 8404.
(110) Bixon, M.; Jortner, *J. Chem. Phys.* **2002**, *281*, 393.
(111) Segal, D.; Nitzan, A. *J. Phys. Chem. B* **2000**, *104*, 3817.
(112) Petrov, E. G.; May, V.; Hanggi, P. *Chem. Phys.* **2002**, *281*, 211.
(113) Weiss, E. A.; Wasielewski, M. R.; Ratner, M. A. *Topics in Current Chemistry*; Springer: Heidelberg, 2005; Vol. 257, p 103.
(114) Berlin, Y. A.; Grozema, F. C.; Siebbeles, L. D. A.; Ratner, M. A. *J. Phys. Chem. C* **2008**, *112*, 10988.
(115) Weiss, E. A.; Tauber, M. J.; Kelley, R. F.; Ahrens, M. J.; Ratner, M. A.; Wasielewski, M. R. *J. Am. Chem. Soc.* **2005**, *127*, 11842.
(116) Goldsmith, R. H.; DeLeon, O.; Wilson, T. M.; Finkelstein-Shapiro, D.; Ratner, M. A.; Wasielewski, M. R. *J. Phys. Chem. A* **2008**, *130*, 4708.
(117) Anariba, F.; McCreery, R. L. *J. Phys. Chem. B* **2002**, *106*, 10355.
(118) McCreery, R. L.; Wu, J.; Kalakodimi, R. P. *Phys. Chem. Chem. Phys.* **2006**, *8*, 2572.
(119) Berlin, Y. A.; Burin, A. L.; Ratner, M. A. *Chem. Phys.* **2002**, *275*, 61.
(120) Xu, B.; Zhange, P.; Li, X.; Tao, N. J. *Nano Lett.* **2004**, *4*, 1105.
(121) Choi, S. H.; Kim, B.; Frisbie, C. D. *Science* **2008**, *320*, 1482.
(122) Zhou, C.; Deshpande, M. R.; Reed, M. A.; Jones, L. I.; Tour, J. M. *Appl. Phys. Lett.* **1997**, *71*, 611.
(123) Chen, J.; Calvet, L. C.; Reed, M. A.; Carr, D. W.; Grubisha, D. S.; Bennett, D. W. *Chem. Phys. Lett.* **1999**, *313*, 741.
(124) Chen, J.; Calvet, L. C.; Reed, M. A.; Carr, D. W.; Grubisha, D. S.; Bennett, D. W. *Chem. Phys. Lett.* **1999**, *313*, 741.
(125) Calvet, L. E.; Wheeler, R. G.; Reed, M. A. *Appl. Phys. Lett.* **2002**, *80*, 1761.
(126) Jeong, S.; Kim, D.; Lee, S.; Park, B.-K.; Moon, J. *Appl. Phys. Lett.* **2006**, *89*, 092101.
(127) Adamec, V.; Calderwood, J. H. *J. Phys. D: Appl. Phys.* **1975**, *8*, 551.

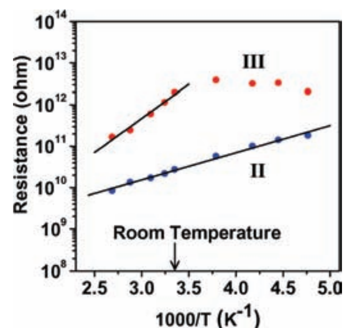

Figure 2. Measurements of SAND electrical resistance in Si/native SiO_2/SAND/Au MIS capacitors, plotted in Arrhenius format for type **II** (blue points) and type **III** (red points) SAND structures. Each point represents the differential resistance in the range ±0.3 and ±0.6 V for types **II** and **III**, respectively.

type **II** and 0.27 ± 0.08 eV for type **III**. The activation energy of **III** is ~2× greater than that of **II**, indicating a larger barrier for the hopping carriers and corresponding to lower leakage current through the film. For a better understanding of the transport differences we have also carefully examined the voltage and electric field dependence of the $I-V$ characteristics. Considering the abrupt apparent change of the transport mechanism around room temperature for type **III**, the remaining results will be divided into two sections corresponding to the low- (−60 to 10 °C) and high-temperature (25−100 °C) regimes.

High-Temperature Transport Regime

The $J-V$ curves of SAND types **II** and **III** were plotted according to the expectations of several transport mechanisms. Schottky injection and Poole−Frenkel emission models were applied to both types of SANDs over the intermediate voltage range (0.0−3.0 V). Since the emission models depend on the permittivity (ε) of the entire dielectric stack, we used the experimental MIS capacitance data reported previously (710 nF/cm^2 for type **II** and 390 nF/cm^2 for type **III**)[34] together with the thicknesses obtained from X-ray reflectivity measurements (**II**, 3.2 nm; **III**, 6.5 nm, Figure S1) in a parallel plate capacitor model ($C = \varepsilon\varepsilon_o A/d$) to extract the ε's of the entire **II**- and **III**-MIS capacitor structures: $\varepsilon = 3.77$ for **II-MIS**, and $\varepsilon = 3.53$ for **III-MIS** (note that the isolated **Stb** layer permittivity is much greater, as discussed in previous publications[34,128]). Using these values in eqs 5 and 6, the barrier heights (ϕ_S and ϕ_{PF}) were varied using nonlinear reduced χ^2 analysis (Origin version 7) to obtain the optimum fit to the experimental data. According to standard regression analysis criteria, an acceptable fit should have an R^2 value greater than 0.95.[129] This criterion allows distinction between Schottky and Poole−Frenkel emission models in describing the experimental $J-V$ data. We find here that the Poole−Frenkel model does not convincingly fit the experimental data ($R^2 = 0.917$) for type **II**, and likewise the Schottky model is not the best fit ($R^2 = 0.968$) to type **III** data. However, Figure 3A and B shows that the best fit for type **II** is the Schottky model (eq 5, $R^2 = 0.985$) and for type **III**, the Poole−Frenkel model (eq 6, $R^2 = 0.999$). The deviation of the nonlinear fits from the experimental data at large voltages (>2.0−2.5 V) strongly suggests a change in mechanism (see Discussion below).

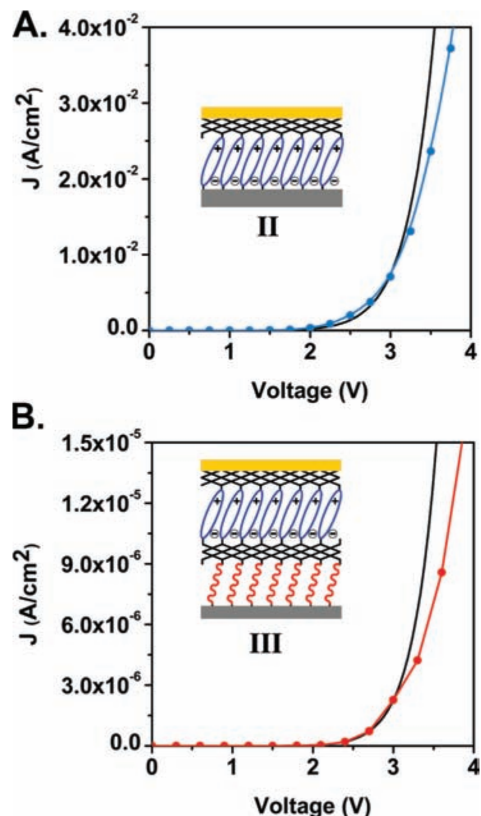

Figure 3. Semilog plots of SAND $J-V$ data with emission model fitting. (A) Experimental data for type **II** (blue points + line) with Schottky emission fit (black solid line). (B) Experimental data for type **III** (red points + line) with Poole−Frenkel fit (black solid line).

More information about transport mechanisms can be obtained by analyzing the $I(V,T)$ data sets in typical emission plots: $\ln(I/T^2)$ vs $1/T$ for Schottky emission (Figure 4) or $\ln(I/V)$ vs $1/T$ for Poole−Frenkel emission (Figure 5).

The physical parameters ε and ϕ_S (ϕ_{PF}) are extracted from the plots in Figures 4B and 5B, where the high-temperature slopes of [$\ln(I/T^2)$ vs $1/T$] (or [$\ln(I/V)$ vs $1/T$]) are plotted against $V^{1/2}$. The thermal barriers ϕ_S (ϕ_{PF}) are determined from the y intercept of the linear regression fit (Origin version 7) in Figures 4B and 5B, and the permittivities of the entire M−SAND−Si stacks can be estimated by solving the β parameter equation $\beta_S = (q^3/4\varepsilon\pi_o\varepsilon)^{1/2}$ (or $\beta_{PF} = (q^3/\varepsilon\pi_o\varepsilon)^{1/2}$) for ε, where β_S (β_{PF}) is the slope of the linear line in Figure 4B (5B). For type **II**, the extracted Schottky barrier is $\phi_S = 0.499 \pm 0.009$ eV and the derived permittivity is $\varepsilon = 2.09 \pm 0.04$. For type **III**, the extracted Poole−Frenkel barrier is $\phi_{PF} = 1.170 \pm 0.022$ eV and the derived permittivity $\varepsilon = 1.92 \pm 0.04$. The parameters derived from the various fits are summarized in Table 1 (see Discussion below). The estimated permittivity values for the **II-MIS** and **III-MIS** stacks are somewhat smaller than the measured values; however, these values are not unphysical (as is sometimes reported in other studies[103,121,130]). Note that when the Poole−Frenkel model is applied to the data for type **II**, the

(128) DiBenedetto, S. A.; Paci, I.; Facchetti, A.; Marks, T. J.; Ratner, M. A. *J. Phys. Chem. B* **2006**, *110*, 22394.
(129) Freund, R. J.; Wilson, W. J. *Regression Analysis: Statistical Modeling of a Response Variable*; Academic Press: San Diego, 1998.
(130) Li, P.; Lu, T.-M. *Phys. Rev. B* **1991**, *43*, 14261.

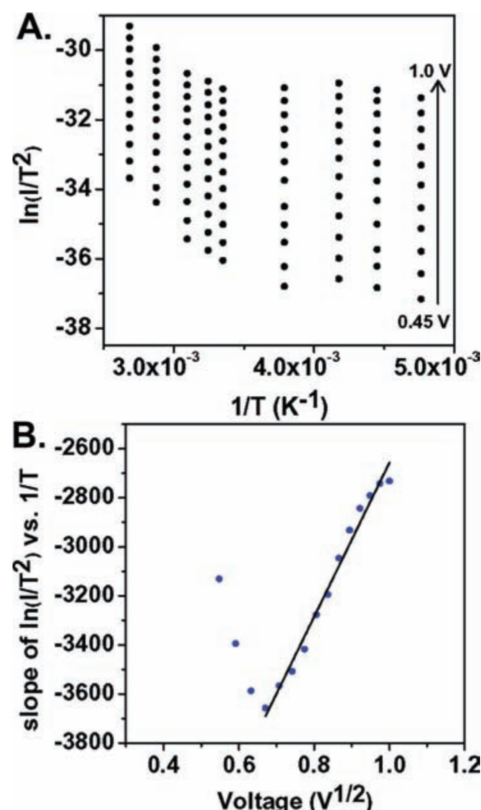

Figure 4. (A) Series of semilog plots of ln(I/T^2) vs 1/T at biases between 0.45 and 1.0 V for SAND type **II**. (B) Plot of the slope of [ln(I/T^2) vs 1/T] vs $V^{1/2}$. The thermal barrier height of the Si/SiO_2/**II**/Au can be deduced from the intercept of the straight line. Note that the units of the y axes are meaningless but the values are arithmetically correct.

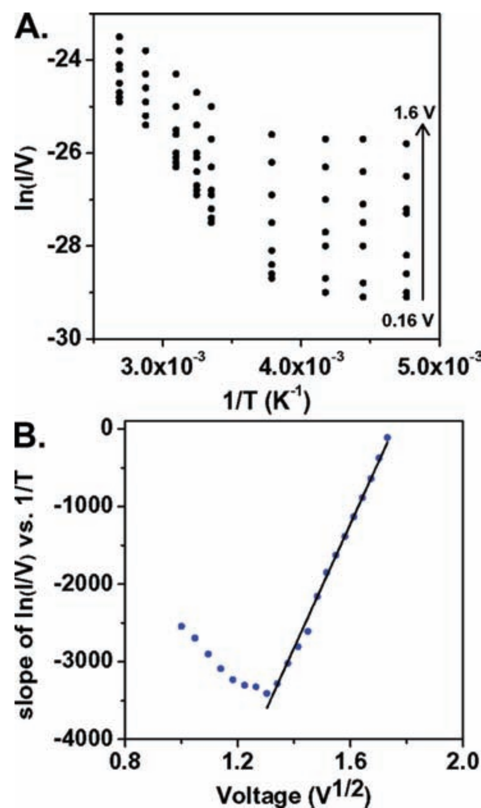

Figure 5. (A) Series of semilog plots of ln(I/V) vs 1/T at biases between 0.16 and 1.6 V for SAND type **III**. (B) Plot of the slope of [ln(I/V) vs 1/T] vs $V^{1/2}$. The thermal barrier height of the Si/SiO_2/**III**/Au can be deduced from the intercept of the straight line. Note that the units of the y axes are meaningless but the values are arithmetically correct.

estimated permittivity is 0.38, and when the Schottky model is applied to the data for type **III**, the estimated permittivity is 9.32. Clearly these values are poorer matches to the experimentally derived permittivity values for the entire Si/SiO_2/SAND/Au stack, and therefore the assignment of the different emission mechanisms in types **II** and **III** (recall the fits in Figures 3A and B) is supported by the reasonable permittivity values obtained.[130] The deviation of the data from the linear fit at low voltages in Figures 4B and 5B is characteristic of hopping transport, already shown in Figure 2.

The deviation of the data from the fits at large voltages in Figures 3A and B is assignable to a change in mechanism to field-induced emission[121] (Fowler−Nordheim tunneling, eq 3). Each curve in the Fowler−Nordheim plots (Figure 6A and B) was collected at a different temperature. For true tunneling behavior, the curves should be indistinguishable (no T dependence in eqs 2 or 3). Figure 6A and B show that MIS devices of SAND types **II** and **III** exhibit typical Fowler-Nordheim behavior at large voltages (to the left of the dashed lines). At lower voltages (to the right of the dashed line) the transport changes to the Schottky emission/hopping regimes described above for type **II**. For SAND type **III**, the region to the right of the dashed line corresponds to the Poole-Frenkel emission mechanism. For SAND type **II**, the evolution to Schottky emission is gradual, whereas for type **III** the change is more striking. The average Fowler−Nordheim tunneling barriers (ϕ_{FN}) are derived from the slopes of linear fits (Origin) to the data in the Fowler−Nordheim regions in

Table 1. Summary of the Derived Energetic Barriers (ϕ, [eV]) Associated with the Various Transport Processes for Si/SiO_2/**II**/Au and Si/SiO_2/**III**/Au SAND-Based MIS Devices and the Corresponding Temperature (T, [°C]) and Voltage (V, [V]) Range[a]

		II		III	
process	T range (°C)	ϕ (eV)	V range (V)	ϕ (eV)	V range (V)
hopping (eq 4)	25−100	0.13	±0.30	0.27	±0.60
Schottky (eq 5)	25−100	0.50	0.3−1.0	NA	NA
P−F (eq 6)	25−100	NA	NA	1.17	0.6−3.0
F−N (eq 3)	−60 to +100	0.65	2.0−3.3	0.85	2.4−4.0
Simmons (eq 7)	−60 to +25	NA	NA	1.42	0.0−2.0
hopping (eq 4)	−60 to +25	0.12	±0.30	0.03	±0.60

[a] P−F = Poole−Frenkel; F−N = Fowler−Nordheim; NA = not applicable.

Figures 6A and B. For type **II**, ϕ_{FN} = 0.65 ± 0.04 eV (between 2.0 and 3.3 V), and for type **III** ϕ_{FN} = 0.85 ± 0.01 eV (between 2.4 and 4.0 V). Additionally, low-voltage tunneling is exhibited by the series of low-temperature $I-V$ scans for **III** (Figure 6B), but not for **II** (Figure 6A). This is consistent with the results shown in Figure 2, and further analysis of the low voltage tunneling observed in type **III** is presented below.

Low-Temperature Transport Regime

The transition from tunneling to hopping/emission is further evaluated by fitting the $I-V$ scans of SAND type **III** at each temperature according the Simmons model (eq 7). The asymmetry of the $I-V$ scans (Figure 7A) most likely reflects the depletion layer in the n^+-Si for negative applied

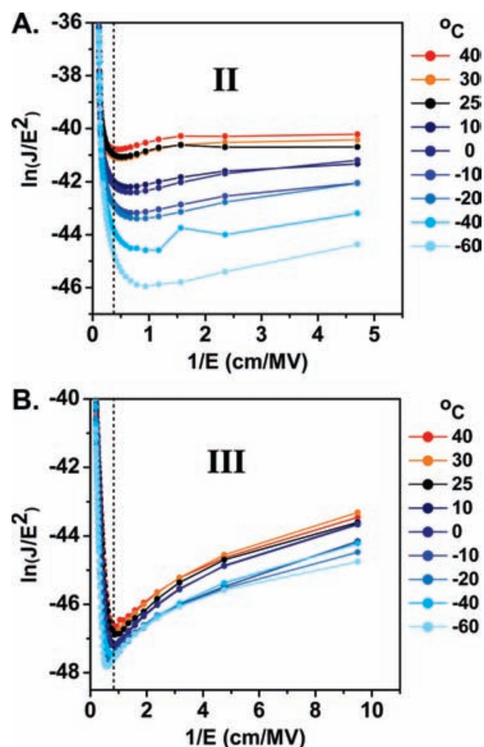

Figure 6. (A) Series of Fowler−Nordheim plots for SAND type **II**. Each line represents a different temperature shown by the legend on the right. (B) Series of Fowler−Nordheim plots for SAND type **III**. Each line represents a different temperature shown by the legend the right.

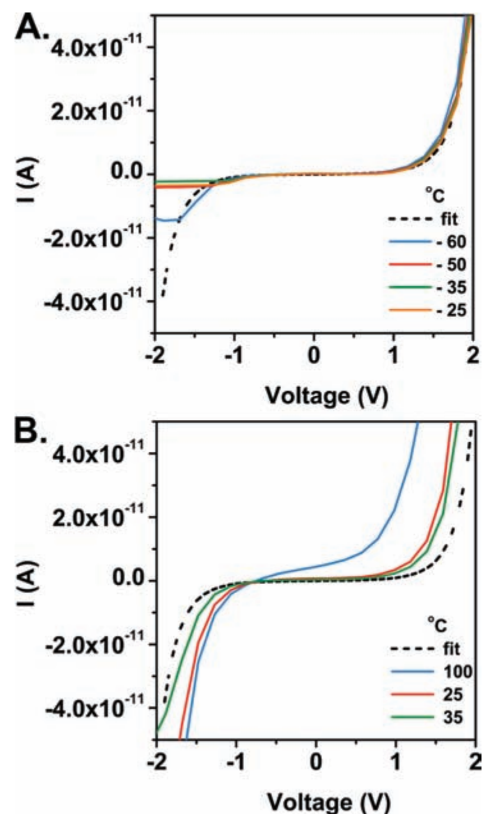

Figure 7. Series of $I-V$ scans collected over a temperature range compared to the best fit of the Simmons model to the −60 °C data (black dashed lines in both A and B). (A) Si/SiO$_2$/**III**/Au over the range of −60 to −25 °C. (B) Si/SiO$_2$/**III**/Au over the range of 25−100 °C.

voltages. Therefore, the tunneling model was fit to the positive applied voltage region with the n^+-Si in accumulation, which corresponds to electron emission from the Si into the SAND. The Simmons model (eq 7)[44] was used to fit the data, where m is the electron mass, $\hbar$ is the reduced Planck's constant, d is the thickness of the film, ϕ_B is the barrier height, V is the applied voltage, and α is a unitless adjustable

$$J = \left(\frac{q}{4\pi^2\hbar d^2}\right)\left\{\left(\phi_B - \frac{qV}{2}\right)\exp\left[-\frac{2(2m)^{1/2}}{\hbar}\alpha\left(\phi_B - \frac{qV}{2}\right)^{1/2}d\right] - \left(\phi_B - \frac{qV}{2}\right)\exp\left[-\frac{2(2m)^{1/2}}{\hbar}\alpha\left(\phi_B + \frac{qV}{2}\right)^{1/2}d\right]\right\} \quad (7)$$

parameter that is introduced to modify the simple rectangular barrier (α = 1), or to account for an effective electron mass. The I(V, T) data can be fit by adjusting the two parameters ϕ_B and α in eq 7.

For type SAND **III**, the −60 °C $I-V$ data can be fit using $\phi_B = 1.429 \pm 0.008$ eV and $\alpha = 0.366 \pm 0.003$ (Figure 7A, black dashed line). Note that the derived fitting parameters ϕ_B and α for an n-CH$_3$(CH$_2$)$_{11}$SH-derived SAM (**C12**) measured in Au−SAM−Au nanopore junctions[44] are very similar (ϕ_B = 1.42 eV and α = 0.65) to those derived for Si/SiO$_2$/SAND-**III**/Au devices in the present study. The similarity between the **C12** and SAND type **III** fitting parameters suggests that at low temperatures the SAND **C8** layer constrains the transport to tunneling, and thus the observation and extraction of tunneling parameters is appropriate (see Discussion below). Each additional curve in Figures 7A and B corresponds to a different temperature $I-V$ scan. Since tunneling is proposed as the low temperature dominant mechanism, each curve measured between −60 and ∼10 °C should track the black dashed fit (without changing the fitting parameters). Figure 7A shows that the entire series of low temperature $I-V$ scans for **III** adheres to the tunneling model, whereas the series of high-temperature $I-V$ scans (Figure 7B) does not. The transition between tunneling to hopping is very abrupt near 25 °C, as shown in Figure 2, supporting the hypothesis that tunneling is the dominant transport mechanism in type **III** SANDs at low temperatures. Note that a Simmons model fit was also attempted for the type **II** SAND data, however the series of $I-V$ scans does not track the model without changing the fitting parameters, again suggesting that the predominant low temperature transport process in type **II** is hopping (Figure 2). Using ϕ_B and α in eq 2, the tunneling efficiency parameter β for type **III** is estimated to be 1.793 Å^{-1}. Such a large β value is indicative of less efficient "through-space" tunneling, where the SAND layer acts as a dielectric medium that modifies the electron transport between the top and bottom electrodes.[45]

Discussion

The observation of different charge conduction mechanisms in SANDs having different structures doubtless reflects the relative magnitudes of the various barriers, as well as the temperature and voltage ranges under consideration. These are compiled in Table 1. It has been demonstrated in OTFTs[34] and in unconventional inorganic TFT devices utilizing SANDs,[131−135] that type **III** SAND is a superior insulator

(131) Hur, S.-H.; Yoon, M.-H.; Gaur, A.; Shim, M.; Facchetti, A.; Marks, T. J.; Rogers, J. A. *J. Am. Chem. Soc.* **2005**, *127*, 13808.

(as evidenced by lower J values, lower TFT V_T's, smaller TFT hysteresis, etc.) than SAND types **I** or **II**. Here the aim is to understand the results by analyzing the differences in transport observed between SAND types **II** and **III** with respect to the constituent structures, temperatures, and applied voltage ranges. Figure 2 shows that transport in SAND type **III** is dominated by two distinct mechanisms: hopping at higher temperatures and tunneling at lower temperatures. The structure of type **III** is composed of two distinctly different molecular layers, σ-saturated **C8** and π-conjugated **Stb**. On the basis of the current understanding of charge transport through saturated vs conjugated SAM(T)s in the molecular electronics field (see the Introduction), it is physically reasonable to assign the ambient temperature hopping behavior to the π-conjugated **Stb** molecular constituent and the tunneling behavior to the σ-saturated **C8** constituent. However, there is a clear transition (at low temperatures) to a temperature-independent process for type **III**. Thus, the major contributor to the leakage current in type **III** SAND below 300 K is due to electrons with significant probability of tunneling from the Si substrate through the **C8**, SiO_2 **Cap**, *and* **Stb** layers. This transition from high-temperature hopping to low-temperature tunneling in π systems is standard behavior in organic materials,[113,115] and is predicted both by formal models[107,111] and by simple physical arguments (the hopping requires activated injection). Considering the multilayered structure of SAND type **III** (including two layers of SiO_2 **Cap**), it is not surprising that the β value estimated here is so much greater than 1.0, as has been observed for other molecular junctions that behave as a dielectric and exhibit through-space tunneling.[45,74,95,136]

As the voltage is increased beyond the low bias hopping regime, the transport mechanisms in types **II** and **III** SANDs change (see Figure 8 below), and different thermal emission models are applicable in describing the leakage currents, as shown in Figures 3−6. This change in charge transport mechanism is of interest because it occurs in the operating voltage range for typical SAND-based TFT devices. For type **II**, between 1.0 and 2.0 V, the current is thermally activated for all temperatures and increases smoothly as the voltage is increased. For type **III**, between ~1.5 and 3.0 V, the high-temperature (>25 °C) $J-V$ curves are thermally activated but the low temperature curves are not, as the current density plots (Figure 8) are shallow and the shape of the $J-V$ plots changes as the voltage is increased. The results in Figures 3−6 collectively show that transport at moderate voltages in the range of 1.0−3.0 V can be understood in terms of electrode dominated Schottky emission for type **II,** and Poole−Frenkel bulk dominated emission for type **III**. The difference in transport between **II** and **III** SANDs is directly correlated with the nanoscale structural differences: where the density of negative charges associated with the **Stb** I^- counterion is located proximate to the n^+-Si surface in type **II** (~1.0 nm above the surface from X-ray standing wave measurements on similar systems[137]) but is separated from the n^+-Si surface by the **C8** layer (and effectively located in the bulk) in type **III**. The location of the charge density is significant in determining the transport mechanism. For typical ionic solids, such as $BaTiO_3$, the energy of the surface states is very close to the conduction/valence band edges.[130,138,139] This suggests that for ionic materials with significant density of charges at the interface, occupation of the surface states is essentially equivalent to occupation of the bands/molecular orbitals, and therefore the surface states do not exhibit a significant energy barrier to charge injection. Thus, the contact between the **Stb** layer and n^+-Si in type **II** is close to an ohmic contact,[130,140,141] and Schottky injection is observed for type **II**, but not for type **III** because the **C8**/n^+-Si contact lacks the density of charges near the interface and behaves as a tunneling barrier. Consequently, the derived injection barrier for type **II** is smaller than for **III** (Table 1), indicating that injection occurs more easily in type **II**. This is intuitively reasonable from (i) the greater thickness of type

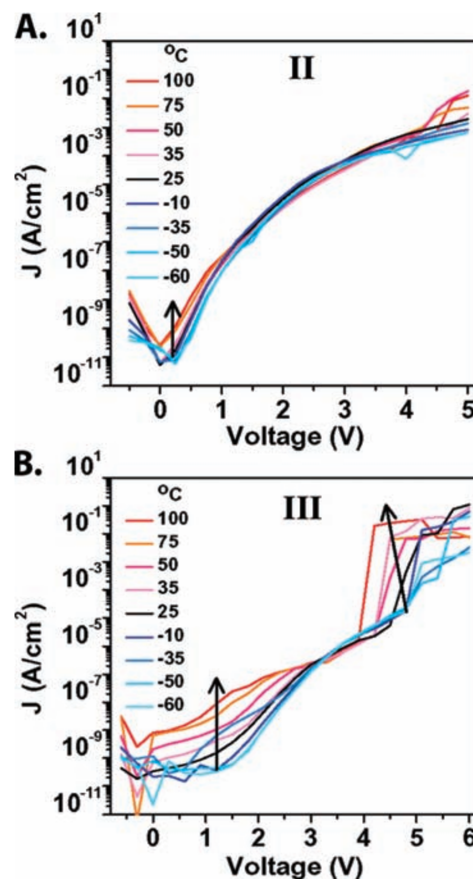

Figure 8. Semilog $J-V$ plots over the entire voltage range for (A) Si/SiO_2/**II**/Au MIS and (B) Si/SiO_2/**III**/Au MIS devices. Each line represents the temperature indicated by the legend, and the arrows indicate direction of increasing temperature.

(132) Wang, L.; Yoon, M.-H.; Lu, G.; Facchetti, A.; Marks, T. J. *Nat. Mater.* **2006**, *5*, 893.
(133) Ju, S.; Lee, K.; Janes, D. B.; Yoon, M.-H.; Facchetti, A.; Marks, T. J. *Nano Lett.* **2005**, *5*, 2281.
(134) Ju, S.; Lee, K.; Janes, D. B.; Dwivedi, R. C.; Abffour-Awuah, H.; Wilkins, R.; Yoon, M.-H.; Facchetti, A.; Marks, T. J. *Appl. Phys. Lett.* **2006**, *89*, 073510.
(135) Ju, S.; Li, J.; Lui, J.; Chen, P.-C.; Ha, Y.-G.; Ishikawa, F.; Change, H.; Zhou, C.; Facchetti, A.; Janes, D. B.; Marks, T. J. *Nano Lett.* **2008**, *8*, 997.
(136) Slowinski, K.; Chamberlain, R. V.; Miller, J.; Majda, M. *J. Am. Chem. Soc.* **1997**, *119*, 11910.
(137) Lin, W.; Lee, T.-L.; Lyman, P. F.; Lee, J.; Bedzyk, M. J.; Marks, T. J. *J. Am. Chem. Soc.* **1997**, *119*, 2205.
(138) Schockley, W. *Phys. Rev.* **1939**, *56*, 317.
(139) Song, J.-H.; Akiyama, T.; Freeman, A. J. *Phys. Rev. B* **2008**, *77*, 035332.
(140) Ratner, M. A. *Mater. Today* **2002**, *5*, 20.
(141) Lee, T.; Chen, N.-P.; Liu, J.; Andres, R. P.; Janes, D. B.; Chen, E. H.; Melloch, M. R.; Woodall, J. M. *Appl. Phys. Lett.* **2000**, *76*, 212.

III, (ii) the smaller homolumo gap of π-conjugated materials compared to σ-saturated materials, and (iii) the larger J of type **II** ($\sim 10^{-6}$ A/cm^2 at 1.0 V) compared to **III** ($\sim 10^{-7}$ A/cm^2 at 2.0 V, Figure 8). Thus, the bulk-dominated transport observed in type **III** results from the combination of both σ- and π-SAMs, exhibiting effective charge blockage that is responsible for the lower leakage currents and enhanced TFT performance.[52,142] Note that these results also help to explain the superior GaAs/GaAs oxide JFET performance when SAND type **III** is used as the surface passivation layer compared to alkyl σ-saturated SAMs (type **I** or ODT).[38]

As the voltage is increased to larger applied biases (corresponding to E fields of $\sim$6 MV/cm), significant quantum mechanical tunneling current (Fowler−Nordheim) is observed in both SANDs **II** and **III**. This high-field stress induces excess leakage current and dielectric breakdown. Voltage induced dielectric breakdown results from a precipitous drop in the resistance of an electrical insulator, although breakdown can also be induced thermally or by mechanical failure.[77] For SAND type **II** it is difficult to distinguish the breakdown event at $\sim$3.2 V ($\sim$6.8 MV/cm, Figure 8) from the normal high current/voltage operation. However for **III**, dielectric breakdown is distinguishable from the Fowler−Nordheim tunneling region (3−4 V) by the rapid spike of the current density at $\sim$4 V (5 MV/cm, Figure 8). These breakdown values are within the range of that measured for Si/SiO$_2$/*n*-octadecyltrichlorosilane/Al (9.5 MV/cm)[143] and a Ag/C8-thiol bilayer/Au-coated AFM junction (5 mV/cm).[144] However, it is known that the dielectric strength depends not only on the conformational order of the dielectric, but also on the thickness of the SAM and the nature of the substrate−dielectric and dielectric−contact interfaces.[92] For example, breakdown strengths of $\sim$4−8 MV/cm (depending on chain length) were measured for alkanethiols on Ag in Ag/SAM/Hg junctions,[145] whereas breakdown strengths as large as 20 MV/cm have been reported for alkyl chains in Au/SAM/Au-coated AFM[144] and Si(111)/SAM/Pt-coated AFM[146] junctions, attesting to the sensitivity to the breakdown measurement methodology. Moreover, breakdown strength can be surprisingly independent of molecular structure,[145] since both σ-saturated and π-conjugated SAMs of the same thicknesses have reported breakdown strengths of 4.0−4.5 MV/cm.[147] Therefore, the larger breakdown strength of type **II** compared to type **III** SANDs is most likely due the location of the charges, which are stabilized[139,148,149] near the electrode in type **II** but are located in the bulk of type **III**. Given that Fowler−Nordheim tunneling is observed at the onset of breakdown in both SAND types, the breakdown can be characterized by different electrical breakdown mechanisms. The catastrophic breakdown event in type **III** at 5 MV/cm can be classified as a 'hard' breakdown, whereas the gradual and noisy breakdown in type **II** at $\sim$7 MV/cm is indicative of a 'soft' breakdown (Figure 8).[150,151] The difference in breakdown mechanism is important for high voltage applications where "graceful" failure (high reliability) is desired because, in these applications, the dielectric is repeatedly exposed to high-field stress.[152,153]

Conclusions

In summary, charge transport mechanisms in type **II** and type **III** SANDs were characterized and analyzed in MIS capacitors. It was found that the position of the **Stb** layer with respect to the Si/SiO$_2$ surface and the inclusion of a tunneling barrier is crucial in controlling the overall leakage currents of SAND structures. Table 1 summarizes the results of the transport mechanism analysis and derived barriers in this study. The first conclusion is that the energy barrier for each transport process is lower for type **II** than for type **III**, which is consistent with the leakage current data—type **II** exhibits larger J values than type **III**. The next major conclusion is that hopping is the dominant transport mechanism at room temperature in both types of SAND-MIS devices. However, there are differences in the transport in SANDs as the temperature and voltage are varied—(i) the resistance as a function of temperature indicates two modes of transport in type **III** but only a single mode in type **II**; (ii) the Schottky emission model fits the data for type **II**, while the Poole−Frenkel emission model best fits the data for type **III**; (iii) the low-temperature $J-V$ curves for type **III** fit the Simmons tunneling model; and finally (iv) the field-induced dielectric breakdown of type **II** is gradual, while that of type **III** is abrupt. These observations can be partly explained by the electronic differences of σ-saturated (**C8**) and π-conjugated (**Stb**) layers at the interface of the injecting electrode (Si/SiO$_2$). The electrode-dominated transport (Schottky emission) observed for type **II** appears to result from the arrangement of **Stb** I^- fixed charges and π-conjugated system directly bound to the Si/SiO$_2$ surface, since the same **Stb** fixed charge is present in type **III** but is separated from the surface by the saturated **C8** SAM. Thus, the lower leakage currents are a major advantage of type **III** and are reasonably due to the **C8** tunneling barrier and additional **Cap** layer. These layers not only reduce the leakage current by blocking injected electrons from the Si, but also shift the transport to the bulk dominated transport regime (Poole−Frenkel). Thus, future SAND-based gate dielectrics for high-performance, low-voltage TFT applications should be designed to resemble type **III**, which enables reduced leakage currents via the order of the σ- and π-layers deposited on the bottom Si electrode, *and* utilizes the large polarizability and dipole moment of the π-conjugated **Stb** molecular constituent. However, device applications requiring high-voltage and high-capacitance may benefit from structures similar to type **II**, where a more favorable breakdown mechanism and higher permittivity is observed.

Acknowledgment. This work was supported by the NSF MRSEC program (DMR-0520513) at the Materials Research Center of Northwestern University and by the ONR MURI

(142) Jeong, D. S.; Hwang, C. S. *J. Appl. Phys.* **2005**, *98*, 113701.
(143) Fontaine, P.; Goguenheim, D.; Deresmes, D.; Vuillaume, D.; Garet, M.; Rondelez, F. *Appl. Phys. Lett.* **1993**, *62*, 2256.
(144) Wold, D. J.; Frisbie, C. D. *J. Am. Chem. Soc.* **2001**, *123*, 5549.
(145) Haag, R.; Rampi, M. A.; Holmlin, R. E.; Whitesides, G. M. *J. Am. Chem. Soc.* **1999**, *121*, 7895.
(146) Zhao, J.; Uosaki, K. *Appl. Phys. Lett.* **2003**, *83*, 2034.
(147) Holmlin, R. E.; Haag, R.; Chabinyc, M. L.; Ismagilov, R. F.; Cohen, A. E.; Terfort, A.; Rampi, M. A.; Whitesides, G. M. *J. Am. Chem. Soc.* **2001**, *123*, 5075.
(148) Kubatkin, S.; Danilov, A.; Hjort, M.; Cornil, J.; Bredas, J.-L.; Stuhr-Hansen, N.; Hedegard, P.; Bjornholm, T. *Nature* **2003**, *425*, 698.
(149) Kaasbjerg, K.; Flensberg, K. *Nano Lett.* **2008**, *8*, 3809.
(150) Baklanov, M.; Green, M.; Maex, K. *Dilectric Films For Advanced Microelectronics*; John Wiley and Sons Ltd.: West Sussex, 2007.
(151) Wolters, D. R.; Verwey, J. F. *Instabilities in Silicon Devices*; Elsevier: Amsterdam, 1986.

Program (N00014-02-1-0909). We thank Dr. M.-H. Yoon for providing SAND samples; Prof. L. Lauhon, Dr. E. Foley (Northwestern University), Dr. E. Furman (Penn State University), and Dr. J. Letizia for helpful discussions on low-noise $I(V,T)$ measurements. We thank Dr. G. Evmenenko and Dr. P. Dutta (Department of Physics, Northwestern University) for helpful discussions about the X-ray reflectivity measurements performed on at Beamline X23B of the National Synchrotron Light Source, which is supported by the U.S. Department of Energy.

Supporting Information Available: X-ray reflectivity spectra and an alternative representation of Figure 2. This material is available free of charge via the Internet at http://pubs.acs.org.

JA9013166

(152) Chu, B.; Zhou, X.; Ren, K.; Neese, B.; Lin, M.; Wang, Q.; Bauer, F.; Zhang, Q. M. *Science* **2006**, *2006*, 334–336.
(153) Claude, J.; Lu, Y.; Wang, Q. *Appl. Phys. Lett.* **2007**, *91*, 212904.